



# Isobutane dehydrogenation over the mesoporous Cr<sub>2</sub>O<sub>3</sub>/Al<sub>2</sub>O<sub>3</sub> catalysts synthesized from a metal-organic framework MIL-101



Huahua Zhao<sup>a,b</sup>, Huanling Song<sup>a,c</sup>, Leilei Xu<sup>a,b</sup>, Lingjun Chou<sup>a,c,\*</sup>

<sup>a</sup> State Key Laboratory for Oxo Synthesis and Selective Oxidation, Lanzhou Institute of Chemical Physics, Chinese Academy of Sciences, Lanzhou 730000, PR China

<sup>b</sup> University of Chinese Academy of Sciences, Beijing 100049, PR China

<sup>c</sup> Suzhou Institute of Nano-Tech and Nano-Bionics, Suzhou 215123, PR China

## ARTICLE INFO

### Article history:

Received 23 November 2012

Received in revised form 1 February 2013

Accepted 16 February 2013

Available online xxx

### Keywords:

Chromia/alumina

Isobutane dehydrogenation

Mesoporous

Metal-organic framework

MIL-101

## ABSTRACT

The reactivity of isobutane dehydrogenation over a series of non-ordered mesoporous chromia/alumina (Cr<sub>2</sub>O<sub>3</sub>/Al<sub>2</sub>O<sub>3</sub>) catalysts with large specific surface area (149.4–381.6 m<sup>2</sup> g<sup>-1</sup>) and high pore volume (0.77–1.24 cm<sup>3</sup> g<sup>-1</sup>), synthesized using a metal-organic framework MIL-101 as a molecular host and chromium precursor, aluminium isopropoxide (Al(*i*-OC<sub>3</sub>H<sub>7</sub>)<sub>3</sub>) as the aluminium precursor, were studied in detail. The chromium species were highly dispersed over the catalyst with chromia loading up to 10 wt.%. The specific surface area of the catalyst decreased, whereas the amount of surface Cr<sup>3+</sup> species and the mole ratio of Cr<sup>3+</sup> and Cr<sup>6+</sup> species (Cr<sup>3+</sup>/Cr<sup>6+</sup>) increased with the increasing chromia loadings (5–25 wt.%) and calcination temperature (500–900 °C), respectively. The addition of potassium to the catalyst system greatly promoted isobutene selectivity and catalyst stability. The catalyst with 1.5 wt.% K<sub>2</sub>O and 10 wt.% Cr<sub>2</sub>O<sub>3</sub> loadings calcined at 800 °C was found to exhibit the highest isobutane conversion 60.1% with the isobutene selectivity up to 93.2% among all the catalysts. The maintainable catalytic reactivity demonstrated the high stability of the catalyst in ten dehydrogenation-regeneration cycles. Moreover, it was proposed that the Cr<sup>3+</sup> species was mainly the active site and catalytic selectivity was depended on the surface Cr<sup>3+</sup>/Cr<sup>6+</sup> value over the catalyst. The catalyst presented much more stable dehydrogenation activity compared with the conventional catalyst. Consequently, this study presents a feasible way to facile synthesis of the mesoporous MOF-derived Cr<sub>2</sub>O<sub>3</sub>/Al<sub>2</sub>O<sub>3</sub> catalysts with high stability and good catalytic reactivity over isobutane dehydrogenation.

© 2013 Elsevier B.V. All rights reserved.

## 1. Introduction

Catalytic dehydrogenation of isobutane over the chromia/alumina (Cr<sub>2</sub>O<sub>3</sub>/Al<sub>2</sub>O<sub>3</sub>) catalyst is an industrially important route for producing isobutene, a vital component for the synthesis of MTBE (methyl tert-butyl ether) and ETBE (ethyl tert-butyl ether), which are increasingly demanded as octane number boosters for unleaded gasoline in the worldwide recently [1–6]. Dehydrogenation is typically performed at relatively high temperatures and low pressures due to thermodynamic requirements. However, reaction conditions, such as high temperature, usually facilitate the thermal cracking and coke formation, thus result in reduced isobutane conversion, decreased isobutene selectivity and severe deactivation of the catalyst [7–9]. It is therefore the key issue to develop catalyst with the ability of possessing high and stable

activity and selectivity and suppressing the coke formation during the catalytic dehydrogenation reaction.

Supported Cr<sub>2</sub>O<sub>3</sub>/Al<sub>2</sub>O<sub>3</sub> catalyst has been applied for the isobutane dehydrogenation on a commercial scale for years [10]. Currently, this catalyst system occupies more than half of the world market of the commercial catalysts for paraffin dehydrogenation [11]. It is well known that the nature of surface chromia is related to the catalytic activity and selectivity. The speciation of surface chromia is strongly depended on the type of the support, the chromium content and calcination treatment [1,2,12–15]. De Rossi et al. reported that Cr<sup>6+</sup> species with minor amount of Cr<sup>5+</sup> species were produced on γ-Al<sub>2</sub>O<sub>3</sub> and silica carriers, whereas Cr<sup>6+</sup> and Cr<sup>5+</sup> species in comparable amounts on the zirconia support [13]. Cavani et al. observed that the relative concentration of surface Cr<sup>3+</sup> and Cr<sup>6+</sup> species increased with the increasing chromia loading. They also found that only Cr<sup>3+</sup> species were produced over the surface of the reduced catalyst [2]. Besides, the researchers have been devoted to improving the catalytic dehydrogenation activity and selectivity as well as the catalyst stability. It has been reported that the addition of alkali metal, such as potassium, to the oxide catalyst system usually promotes the catalytic selectivity of olefins and improves

\* Corresponding author at: State Key Laboratory for Oxo Synthesis and Selective Oxidation, Lanzhou Institute of Chemical Physics, Chinese Academy of Sciences, Lanzhou 730000, PR China. Tel.: +86 0931 4968066; fax: +86 0931 4968129.

E-mail address: [ljchou@licp.cas.cn](mailto:ljchou@licp.cas.cn) (L. Chou).

the resistance of the catalyst to deactivation [2,6,16–22]. Many preparation methods for the  $\text{Cr}_2\text{O}_3/\text{Al}_2\text{O}_3$  catalysts described in the literatures, such as incipient wetness impregnation, atomic layer epitaxy (ALE), co-precipitation method and evaporation-induced self-assembly (EISA) strategy, have been explored over the alkanes dehydrogenation [2,7,15,23,24]. However, the utilization of the method that the precursor containing aluminium source impregnated into the Cr-based framework to prepare the  $\text{Cr}_2\text{O}_3/\text{Al}_2\text{O}_3$  catalyst for isobutane dehydrogenation has been paid little attention so far. The similar reports for this method were employed to prepare the nickel catalysts in the reaction of methane decomposition [25–27]. This method may be contributable to a high dispersion of chromium species over the support.

MIL-101 ( $\text{Cr}_3\text{F}(\text{H}_2\text{O})_2\text{O}(\text{BDC})_3 \cdot n\text{H}_2\text{O}$ ,  $n \approx 25$ , MIL = Matériel Institut Lavoisier, BDC = 1,4-benzenedicarboxylate) is one of the porous Cr-based metal-organic frameworks (MOFs). It has a large Brunauer–Emmett–Teller (BET) specific surface area about  $4100 \text{ m}^2 \text{ g}^{-1}$  and high pore volume about  $2.0 \text{ cm}^3 \text{ g}^{-1}$  [28–31]. Its two large mesopores with 2.9 and 3.4 nm pore diameters together with its considerable chromium content (21.7%) stimulate us to prepare the mesoporous  $\text{Cr}_2\text{O}_3/\text{Al}_2\text{O}_3$  catalyst using it as a molecular flask and chromium precursor [32–35]. In the current work, the mesoporous  $\text{Cr}_2\text{O}_3/\text{Al}_2\text{O}_3$  catalyst with large specific surface area and high pore volume was synthesized by utilizing the MIL-101 framework as a molecular host and chromium precursor, aluminium isopropoxide ( $\text{Al}(i\text{-OC}_3\text{H}_7)_3$ ) as the aluminium precursor. The chromia loadings, addition of potassium oxide ( $\text{K}_2\text{O}$ ) and calcination temperature of the catalyst were investigated in detail over the isobutane dehydrogenation. The high isobutene selectivity 93.2% at the high isobutane conversion of 60.1% was obtained in the experiment. In order to study the stability and regenerative ability of the catalyst, the ten dehydrogenation-regeneration cycles were carried out.

## 2. Experimental

### 2.1. Materials

1,4-Benzene dicarboxylic acid ( $\text{H}_2\text{BDC}$ ,  $\text{C}_8\text{H}_6\text{O}_4$ ,  $\geq 98.0\%$ ) and aluminium isopropoxide ( $\text{Al}(i\text{-OC}_3\text{H}_7)_3$ ,  $\geq 98.0\%$ ) were purchased from Sigma–Aldrich (USA). Chromium nitrate nonahydrate ( $\text{Cr}(\text{NO}_3)_3 \cdot 9\text{H}_2\text{O}$ ,  $\geq 99.0\%$ ), hydrofluoric acid (HF,  $\geq 40.0\%$ ), potassium hydroxide (KOH,  $\geq 82.0\%$ ) and absolute ethanol (EtOH,  $\geq 99.7\%$ ) were from Sinopharm Chemical Reagent Co., Ltd (China). The industrial  $\gamma\text{-Al}_2\text{O}_3$  ( $S_{\text{BET}} = 332.3 \text{ m}^2 \text{ g}^{-1}$ ) was purchased from Guizhou Aluminium Corporation (China). All the materials were used as received from vendors without further purification.

### 2.2. Catalysts synthesis

MIL-101 was synthesized by the solvothermal method according to the previous literature with the exception that the mole ratio of  $n(\text{Cr}(\text{NO}_3)_3 \cdot 9\text{H}_2\text{O}) : n(\text{H}_2\text{BDC}) : n(\text{HF}) : n(\text{H}_2\text{O})$  was 1:1:0.5:280 [36]. The as-synthesized MIL-101 was degassed under reduced pressure at  $150^\circ\text{C}$  for 12 h to remove the guest molecules. The pretreated MIL-101 (0.56 g) was added into absolute ethanol (EtOH) solution containing  $\text{Al}(i\text{-OC}_3\text{H}_7)_3$  ( $0.30 \text{ mol L}^{-1}$ , 100 mL) and impregnated by ultrasonic for 1.5 h. Afterwards, the mixture was stirred at  $50^\circ\text{C}$  to evaporate slowly the solvent to form a green paste. The paste was dried at  $120^\circ\text{C}$  overnight to obtain a bright green powder, which was calcined at  $600^\circ\text{C}$  for 4 h in air to obtain the catalyst, denoted as  $10\text{Cr}_2\text{O}_3/\text{Al}_2\text{O}_3(600)$ . The catalysts  $x\text{Cr}_2\text{O}_3/\text{Al}_2\text{O}_3(600)$  ( $x$  wt.% stands for the weight ratio of  $\text{Cr}_2\text{O}_3$  loading in the catalysts and the number in parentheses represents for the calcination

temperature) with different  $\text{Cr}_2\text{O}_3$  loadings (5–25 wt.%) were prepared through controlling the addition amount of MIL-101.

To examine the additive  $\text{K}_2\text{O}$  over the reactivity of isobutane dehydrogenation, KOH (0.04 g) together with  $\text{Al}(i\text{-OC}_3\text{H}_7)_3$  was dissolved in EtOH solution according to the preparation steps of the catalyst  $10\text{Cr}_2\text{O}_3/\text{Al}_2\text{O}_3(600)$  mentioned above to obtain the catalyst  $1.5\text{K}_2\text{O}-10\text{Cr}_2\text{O}_3/\text{Al}_2\text{O}_3(600)$  with 1.5 wt.%  $\text{K}_2\text{O}$  loading.

In order to investigate the calcination temperature over the catalytic activity and selectivity of isobutane dehydrogenation, the catalyst  $1.5\text{K}_2\text{O}-10\text{Cr}_2\text{O}_3/\text{Al}_2\text{O}_3(\text{T})$  (T stands for the calcination temperatures) was calcined at  $500^\circ\text{C}$ ,  $600^\circ\text{C}$ ,  $700^\circ\text{C}$ ,  $800^\circ\text{C}$  and  $900^\circ\text{C}$ , respectively.

The reference alumina supported chromia catalyst  $1.5\text{K}_2\text{O}-10\text{Cr}_2\text{O}_3/\text{Al}_2\text{O}_3(800)\text{-R}$  was prepared by impregnation method and described as follows: KOH (0.04 g) and  $\text{Cr}(\text{NO}_3)_3 \cdot 9\text{H}_2\text{O}$  (0.90 g) were dissolved in EtOH solvent (100 mL). After adding  $\gamma\text{-Al}_2\text{O}_3$  (1.53 g), the mixture was stirred at  $50^\circ\text{C}$  to evaporate slowly the solvent to form a green paste. The following preparation steps were the same as those of the catalyst  $1.5\text{K}_2\text{O}-10\text{Cr}_2\text{O}_3/\text{Al}_2\text{O}_3(800)$ .

### 2.3. Catalytic tests

The reactivity of the each catalyst over isobutane dehydrogenation was carried out in a continuous flow reactor consisting of a fixed-bed quartz tube at  $600^\circ\text{C}$ . The each catalyst (0.60 g, 60–80 mesh) was loaded in the reactor supported on the quartz sand, then heated to the set temperature under the  $\text{N}_2$  flow. The isobutane was fed into the reactor during 5 min. The reaction products were analyzed for 2 h time-on-stream (TOS) with gas chromatography. The original green colour over the fresh catalysts was changed to the black one after the isobutane dehydrogenation. In case of the ten dehydrogenation-regeneration cycles, the catalyst  $1.5\text{K}_2\text{O}-10\text{Cr}_2\text{O}_3/\text{Al}_2\text{O}_3(800)$  was regenerated under air at  $650^\circ\text{C}$  for 2 h and cooled down to room temperature, then utilized to the next cycle.

### 2.4. Characterizations

Powder X-ray diffraction measurements (PXRD) of the products were performed on an X-ray diffractometer (PANalytical) by using Ni-filtered  $\text{Cu K}\alpha$  radiation ( $\lambda = 0.15418 \text{ nm}$ ) from 0.6 to  $5.0^\circ$  (small angle range) and 20.0 to  $80.0^\circ$  (wide angle range).

The  $\text{N}_2$  adsorption–desorption isotherms were detected on a Quantachrome autosorb iQ gas-sorption apparatus at  $-196^\circ\text{C}$ . All samples except MIL-101 (evacuated at  $150^\circ\text{C}$  for 6 h) were activated by degassing in situ under vacuum at  $200^\circ\text{C}$  for 4 h prior to the measurements. BET specific surface areas of the samples were estimated over the relative pressure range of 0.05–0.30. The pore size of MIL-101 was calculated according to the Non-Local Density Functional Theory (NLDFT) and the pore sizes of the catalysts were calculated based on the Barrett–Joiner–Halenda (BJH) method.

The products were subjected to the transmission electron microscopy (TEM) analysis on the FEI TECNAI  $\text{G}^2$  instrument operated at 200 kV.

Ultraviolet–visible spectroscopy (UV–vis) of the samples was collected on a PE Lambda 650S instrument coupled with a diffuse reflectance accessory.

X-ray photoelectron spectroscopy (XPS) of the products was carried out on a VG ESCALAB 250 apparatus equipped with Al  $\text{K}\alpha$  and Mg  $\text{K}\alpha$  X-ray source and a hemispheric analyzer. The binding energies were referenced to the C 1s peak from the carbon surface deposit at 284.8 eV.

Temperature programmed reduction (TPR) measurements for the products with  $\text{H}_2$  as the reducing agent were monitored on a thermal conductivity detector (TCD) cell (TP-5080). Prior to the reduction steps, samples were pretreated at  $300^\circ\text{C}$  for 0.5 h in flowing He ( $30 \text{ mL min}^{-1}$ ) to remove any moisture and other impurities

**Table 1**  
The textural data of the catalysts.

Sample	$S_{\text{BET}}$ ( $\text{m}^2 \text{g}^{-1}$ )	$V_p$ ( $\text{cm}^3 \text{g}^{-1}$ )	$D_p$ (nm)
5Cr <sub>2</sub> O <sub>3</sub> /Al <sub>2</sub> O <sub>3</sub> (600)	381.6	1.21	9.52
10Cr <sub>2</sub> O <sub>3</sub> /Al <sub>2</sub> O <sub>3</sub> (600)	375.6	1.24	9.55
15Cr <sub>2</sub> O <sub>3</sub> /Al <sub>2</sub> O <sub>3</sub> (600)	324.6	1.21	12.32
20Cr <sub>2</sub> O <sub>3</sub> /Al <sub>2</sub> O <sub>3</sub> (600)	267.1	0.78	7.79
25Cr <sub>2</sub> O <sub>3</sub> /Al <sub>2</sub> O <sub>3</sub> (600)	237.0	1.09	12.30
1.5 K <sub>2</sub> O-10Cr <sub>2</sub> O <sub>3</sub> /Al <sub>2</sub> O <sub>3</sub> (500)	337.2	1.17	9.54
1.5 K <sub>2</sub> O-10Cr <sub>2</sub> O <sub>3</sub> /Al <sub>2</sub> O <sub>3</sub> (600)	334.8	1.04	9.54
1.5 K <sub>2</sub> O-10Cr <sub>2</sub> O <sub>3</sub> /Al <sub>2</sub> O <sub>3</sub> (700)	264.7	1.08	12.29
1.5 K <sub>2</sub> O-10Cr <sub>2</sub> O <sub>3</sub> /Al <sub>2</sub> O <sub>3</sub> (800)	197.6	0.87	16.93
1.5 K <sub>2</sub> O-10Cr <sub>2</sub> O <sub>3</sub> /Al <sub>2</sub> O <sub>3</sub> (900)	149.4	0.77	17.22
1.5 K <sub>2</sub> O-10Cr <sub>2</sub> O <sub>3</sub> /Al <sub>2</sub> O <sub>3</sub> (800) <sup>a</sup>	190.9	0.65	12.28
1.5 K <sub>2</sub> O-10Cr <sub>2</sub> O <sub>3</sub> /Al <sub>2</sub> O <sub>3</sub> (800) <sup>b</sup>	177.9	0.55	12.29
1.5 K <sub>2</sub> O-10Cr <sub>2</sub> O <sub>3</sub> /Al <sub>2</sub> O <sub>3</sub> (800) <sup>c</sup>	172.1	0.53	9.55
1.5 K <sub>2</sub> O-10Cr <sub>2</sub> O <sub>3</sub> /Al <sub>2</sub> O <sub>3</sub> (800)-R	234.3	0.29	3.41

<sup>a,b,c</sup> stand for the corresponding spent, first and tenth regenerated catalyst, respectively.

that may be present. After cooling the reactor to room temperature, the sample (50 mg) was loaded in a quartz reactor, then heated to 800 °C at a rate of 10 °C min<sup>-1</sup> under a flow of 5% H<sub>2</sub>-Ar (30 mL min<sup>-1</sup>) gas mixture.

### 3. Results and discussion

#### 3.1. The preparation of the mesoporous Cr<sub>2</sub>O<sub>3</sub>/Al<sub>2</sub>O<sub>3</sub> catalysts

The preparation procedure of the mesoporous Cr<sub>2</sub>O<sub>3</sub>/Al<sub>2</sub>O<sub>3</sub> catalysts is suggested in Scheme S1 (See the supporting information). The Al(*i*-OC<sub>3</sub>H<sub>7</sub>)<sub>3</sub> molecules go into the framework of MIL-101 by adsorption and diffusion with ultrasonic impregnation method to obtain a composite precursor. Then the precursor is directly calcined at a set temperature by decomposing the organic part to produce the Cr<sub>2</sub>O<sub>3</sub>/Al<sub>2</sub>O<sub>3</sub> catalysts.

#### 3.2. The characterizations of the fresh catalysts

##### 3.2.1. Textural analysis

The N<sub>2</sub> adsorption-desorption isotherms and pore size distributions for the two series fresh catalysts xCr<sub>2</sub>O<sub>3</sub>/Al<sub>2</sub>O<sub>3</sub>(600) and 1.5 K<sub>2</sub>O-10Cr<sub>2</sub>O<sub>3</sub>/Al<sub>2</sub>O<sub>3</sub>(T) are shown in Fig. S1. Hysteresis loops between adsorption and desorption branches can be observed for all the catalysts, which demonstrated the existence of mesopores. Table 1 summarizes the textural data of the catalysts. The average pore sizes of the catalysts were located between 7.79 nm and 17.22 nm, clearly demonstrated its mesoporosity. It can be noticeably seen that the xCr<sub>2</sub>O<sub>3</sub>/Al<sub>2</sub>O<sub>3</sub>(600) catalysts with large BET specific surface areas (237.0–381.6 m<sup>2</sup> g<sup>-1</sup>) and high pore volumes (0.78–1.24 cm<sup>3</sup> g<sup>-1</sup>) were obtained with this method, which were much higher than that of the mesoporous Cr<sub>2</sub>O<sub>3</sub>/Al<sub>2</sub>O<sub>3</sub> catalysts prepared with EISA strategy reported by Shee et al. [24]. For the series xCr<sub>2</sub>O<sub>3</sub>/Al<sub>2</sub>O<sub>3</sub>(600) catalysts, the BET specific surface area decreased from 381.6 m<sup>2</sup> g<sup>-1</sup> to 237.0 m<sup>2</sup> g<sup>-1</sup> as the chromia loading increased from 5 wt.% to 25 wt.%. This was due to that the small chromia particles gradually aggregated to large ones over the surface of the catalyst with the increase of Cr<sub>2</sub>O<sub>3</sub> loading, thus blocking a portion of pores and resulting in the decrease of the specific surface area of the catalyst. The pore size distribution of the catalyst became broader and the pore size of the catalyst grew larger from 9.52 nm to 12.32 nm as the Cr<sub>2</sub>O<sub>3</sub> loading increased from 5 wt.% to 15 wt.%, which were probably due to that the porous MIL-101 framework had some influence over the pore structure of the catalyst.

After K<sub>2</sub>O was introduced to the catalyst system, both the BET specific surface area 375.6 m<sup>2</sup> g<sup>-1</sup> and pore volume 1.24 cm<sup>3</sup> g<sup>-1</sup> of

the catalyst 10Cr<sub>2</sub>O<sub>3</sub>/Al<sub>2</sub>O<sub>3</sub>(600) slightly declined to 334.8 m<sup>2</sup> g<sup>-1</sup> and 1.04 cm<sup>3</sup> g<sup>-1</sup> over the one 1.5 K<sub>2</sub>O-10Cr<sub>2</sub>O<sub>3</sub>/Al<sub>2</sub>O<sub>3</sub>(600). Nevertheless, the addition of K<sub>2</sub>O had no remarkable influence over the pore size (9.54 nm) of the catalyst, which indicated that introduction of K<sub>2</sub>O caused no pore plugging of the mesoporous Cr<sub>2</sub>O<sub>3</sub>/Al<sub>2</sub>O<sub>3</sub> catalyst.

In case of the series catalysts 1.5 K<sub>2</sub>O-10Cr<sub>2</sub>O<sub>3</sub>/Al<sub>2</sub>O<sub>3</sub>(T) calcined at different temperatures, 1.5 K<sub>2</sub>O-10Cr<sub>2</sub>O<sub>3</sub>/Al<sub>2</sub>O<sub>3</sub>(500) possessed the largest BET specific surface area (337.2 m<sup>2</sup> g<sup>-1</sup>) and highest pore volume (1.17 cm<sup>3</sup> g<sup>-1</sup>). It was observed that both the BET specific surface area and pore volume of the catalyst became smaller and the pore size gradually grew larger at the calcination temperature from 500 °C to 900 °C. Moreover, the pore size distribution of the catalyst grew broader with increasing calcination temperature (especially calcined at 800 °C and 900 °C, respectively). The phenomenon was probably ascribed to that a small portion of the pores went collapsed at high calcination temperature. By contrast with the reference catalyst (234.3 m<sup>2</sup> g<sup>-1</sup>), the catalyst 1.5 K<sub>2</sub>O-10Cr<sub>2</sub>O<sub>3</sub>/Al<sub>2</sub>O<sub>3</sub>(800) showed a smaller specific surface area 190.9 m<sup>2</sup> g<sup>-1</sup>.

##### 3.2.2. PXRD patterns

The PXRD patterns for the series fresh xCr<sub>2</sub>O<sub>3</sub>/Al<sub>2</sub>O<sub>3</sub> catalysts are presented in Fig. 1A. No diffraction peaks are revealed in the small angle range (0.6–5°) of the series xCr<sub>2</sub>O<sub>3</sub>/Al<sub>2</sub>O<sub>3</sub> catalysts (not show), indicating their non-ordered pore structure. The crystalline chromia phase was not visible in the PXRD patterns until the chromia loading was up to 15 wt.%, suggesting that the sizes of chromia particles were very small and the particles were highly dispersed at least up to 10 wt.% loading on the alumina support [12]. Furthermore, the three broad and weak peaks at 2θ = 37.5°, 45.6° and 66.5° indicated the appearance of the crystalline γ-Al<sub>2</sub>O<sub>3</sub> phase in the support. However, the phase of alumina support was mainly the amorphous phase calcined at 600 °C.

The PXRD patterns of the fresh catalysts 1.5 K<sub>2</sub>O-10Cr<sub>2</sub>O<sub>3</sub>/Al<sub>2</sub>O<sub>3</sub>(T) calcined at different temperatures are described in Fig. 1B. Similar to the catalysts above, no peak signals were observed in the small angle range for the series catalysts (not given), also implying their non-ordered pore structures. K<sub>2</sub>O phase was not revealed in the PXRD pattern of the K-doped catalyst, clearly demonstrating that potassium species were highly dispersed on the alumina support and had no significant influence over the phase of the catalyst. Moreover, the crystalline Cr<sub>2</sub>O<sub>3</sub> phase was not visible in the PXRD patterns of all the catalysts, indicating that chromia species were highly dispersed and the calcination temperature did not affect the dispersion of the chromia species. Simultaneously, it was observed that the characteristic peak shape and intensity of γ-Al<sub>2</sub>O<sub>3</sub> phase in the PXRD patterns became sharper and stronger with the higher calcination temperature, suggesting that the support calcined at the higher temperature possessed the pore wall with more crystalline γ-Al<sub>2</sub>O<sub>3</sub> phase. However, another crystalline phase α-Al<sub>2</sub>O<sub>3</sub> was visible in the catalyst 1.5 K<sub>2</sub>O-10Cr<sub>2</sub>O<sub>3</sub>/Al<sub>2</sub>O<sub>3</sub>(900), implying that γ-Al<sub>2</sub>O<sub>3</sub> phase was partly transformed to α-Al<sub>2</sub>O<sub>3</sub> phase at 900 °C.

##### 3.2.3. TEM images

It was very difficult to obtain the clear TEM images due to the samples were extremely sensitive to the electron beam and the structure collapsed after a few minutes. However, the TEM images of the fresh catalysts in Fig. 2a–f can show their pore structures. In accordance with the N<sub>2</sub> adsorption-desorption characterization, the pore size appeared to be 9 nm, 10 nm, 12 nm, 17 nm and 17.5 nm over the catalysts 1.5 K<sub>2</sub>O-10Cr<sub>2</sub>O<sub>3</sub>-Al<sub>2</sub>O<sub>3</sub>(T) calcined at 500 °C, 600 °C, 700 °C, 800 °C and 900 °C, respectively. The worm-like mesopore structure suggested the absence of the long-range

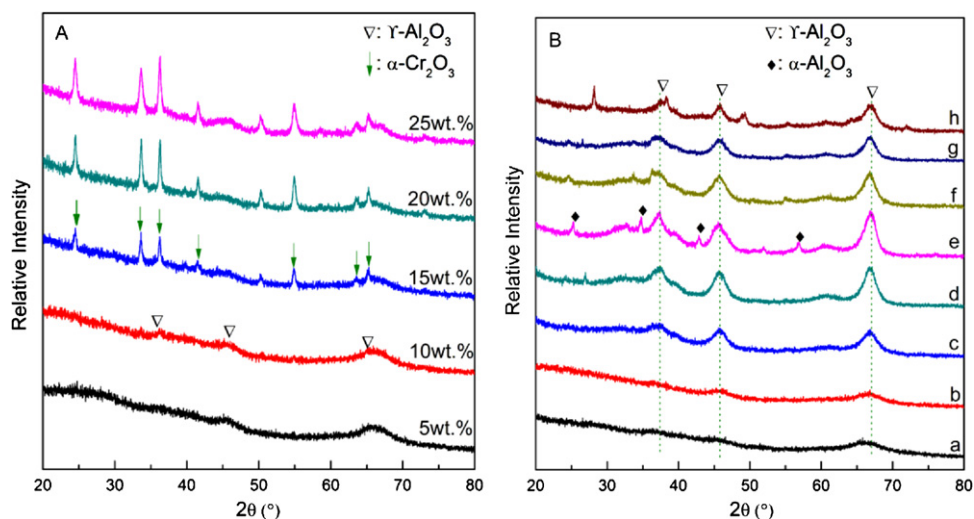


**Fig. 1.** The PXRD patterns of the series fresh catalysts (A)  $x\text{Cr}_2\text{O}_3/\text{Al}_2\text{O}_3$ ; (B)  $1.5\text{K}_2\text{O}-10\text{Cr}_2\text{O}_3/\text{Al}_2\text{O}_3(\text{T})$  calcined at (a) 500 $^\circ\text{C}$  (b) 600 $^\circ\text{C}$  (c) 700 $^\circ\text{C}$  (d) 800 $^\circ\text{C}$  (e) 900 $^\circ\text{C}$  (f) the spent and (g) the tenth regenerated one  $1.5\text{K}_2\text{O}-10\text{Cr}_2\text{O}_3/\text{Al}_2\text{O}_3(800)$  (h) the reference one  $1.5\text{K}_2\text{O}-10\text{Cr}_2\text{O}_3/\text{Al}_2\text{O}_3(800)\text{-R}$ .

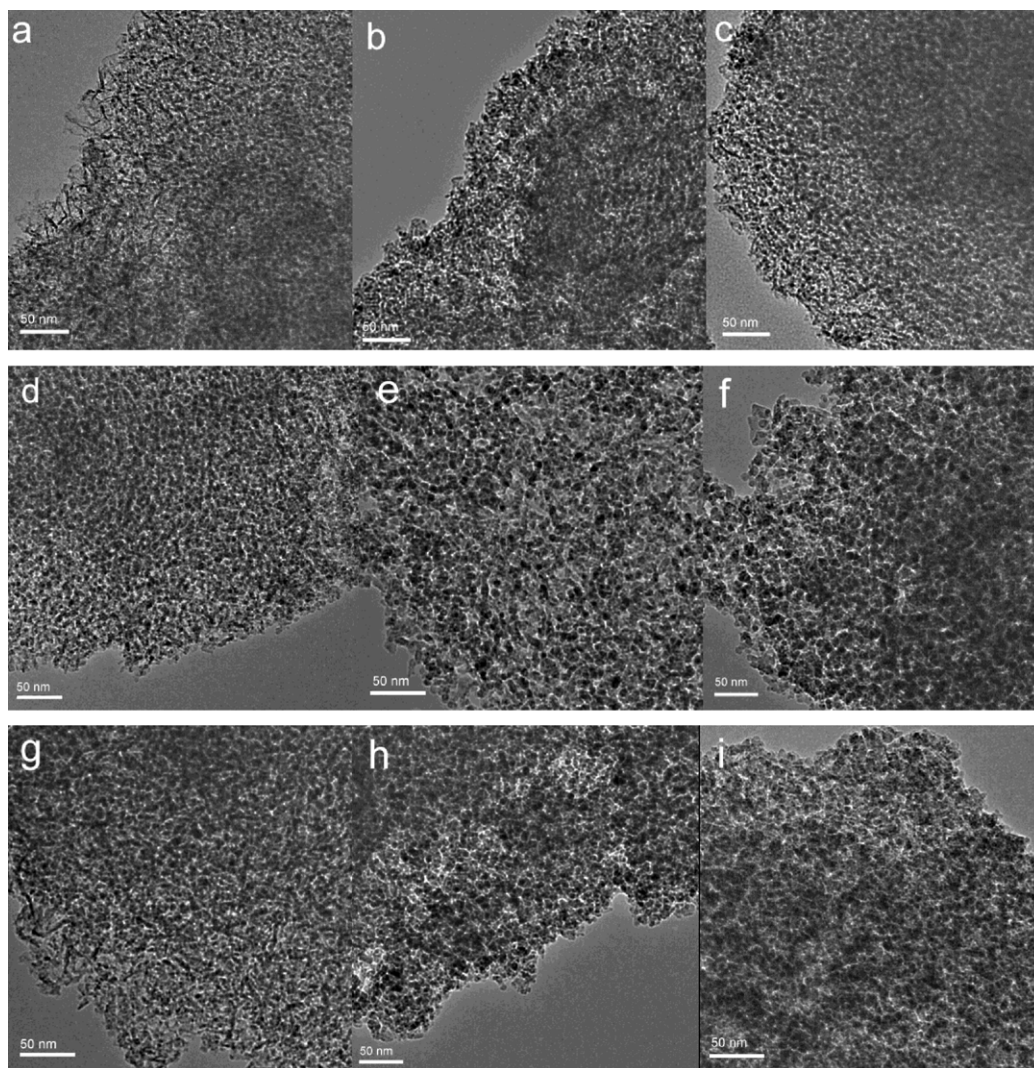


**Fig. 2.** The TEM images of the fresh catalysts (a)  $10\text{Cr}_2\text{O}_3/\text{Al}_2\text{O}_3(600)$  and  $1.5\text{K}_2\text{O}-10\text{Cr}_2\text{O}_3/\text{Al}_2\text{O}_3(\text{T})$  calcined at (b) 500 $^\circ\text{C}$  (c) 600 $^\circ\text{C}$  (d) 700 $^\circ\text{C}$  (e) 800 $^\circ\text{C}$  (f) 900 $^\circ\text{C}$  and the spent ones (g)  $10\text{Cr}_2\text{O}_3/\text{Al}_2\text{O}_3(600)$  (h)  $1.5\text{K}_2\text{O}-10\text{Cr}_2\text{O}_3/\text{Al}_2\text{O}_3(800)$  (i)  $1.5\text{K}_2\text{O}-10\text{Cr}_2\text{O}_3/\text{Al}_2\text{O}_3(800)$  after ten dehydrogenation-regeneration cycles.

uniform pore channels, which were well consistent with their PXRD results. It was noticeably seen that no extra nanoparticles were over the catalysts, indicating that potassium and chromia species were both highly dispersed on all the catalysts and the addition of  $K_2O$  had no marked influence over the pore structures of the catalysts.

### 3.2.4. XPS spectra

Table 2 summarizes the XPS data for the studied catalysts. The Cr 2p<sub>3/2</sub> XPS spectra of the samples divided by fitting the doublet peaks are described in Fig. S2. The bands were located at the binding energy (BE) = 576.5–577.4 eV and 579.4–580.3 eV, which were attributed to  $Cr^{3+}$  and  $Cr^{6+}$  species, respectively [2,14,37–40]. As expected, the total amount of surface chromium enhanced from 1.46% to 4.81% with the increasing chromia loading for the series catalysts  $xCr_2O_3/Al_2O_3(600)$ . The mole ratio of  $Cr^{3+}$  and  $Cr^{6+}$  ( $Cr^{3+}/Cr^{6+}$ ) increased from 1.30 to 2.05 over the catalyst with chromia loading from 5 wt.% to 20 wt.%. Nevertheless, the  $Cr^{3+}/Cr^{6+}$  value decreased to 1.57 over the catalyst  $25Cr_2O_3/Al_2O_3(600)$ . It was calculated that the amounts of surface  $Cr^{3+}$  and  $Cr^{6+}$  species both increased with the increasing chromia loading, whereas the amount of  $Cr^{3+}$  species increased more greatly than that of  $Cr^{6+}$  species over the surface of the series catalysts up to 20 wt.% chromia loading.

The addition of  $K_2O$  to the catalyst system led to the total amount of surface Cr species increasing slightly from 1.78% to 2.01%. The  $Cr^{3+}/Cr^{6+}$  value, however, decreased largely from 1.68 to 1.16. It was observed that the amount of surface  $Cr^{3+}$  species decreased slightly and the amount of surface  $Cr^{6+}$  species increased dramatically upon the  $K_2O$  addition to the catalyst, which indicated that  $K_2O$  could stabilize the  $Cr^{6+}$  species mainly at the expense of the inner  $\alpha-Cr_2O_3$  phase [2,20].

In case of the series catalysts  $1.5K_2O-10Cr_2O_3/Al_2O_3(T)$ , the total surface chromium and potassium amounts of the catalyst gradually increased with the calcination temperature from 500 °C to 900 °C, which was probably due to that the abatement in specific surface area of the catalyst resulted in the decline for the dispersion of chromium and potassium species over the catalyst. The surface  $Cr^{3+}/Cr^{6+}$  value was 0.87 over the catalyst  $1.5K_2O-10Cr_2O_3/Al_2O_3(500)$ , demonstrating that the amount of  $Cr^{6+}$  species was more than that of  $Cr^{3+}$  species over the surface of the catalyst calcined at 500 °C. However, the  $Cr^{3+}/Cr^{6+}$  value increased from 1.16 to 2.57 with the calcination temperature increasing from 600 °C to 900 °C, indicating that  $Cr^{3+}$  gradually became the

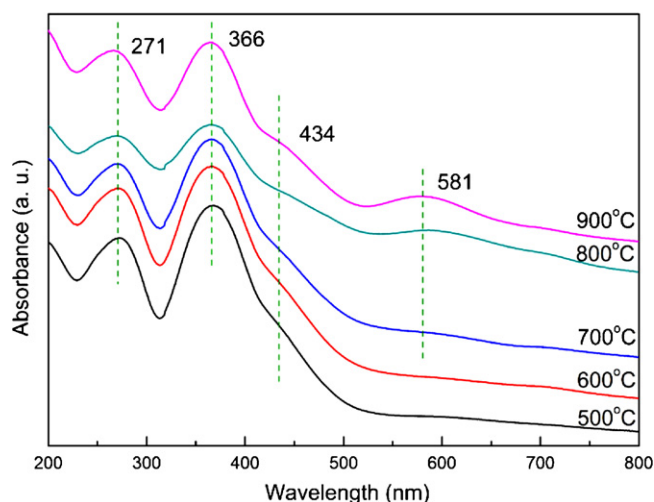


Fig. 3. The UV-vis spectra of the series fresh catalysts  $1.5K_2O-10Cr_2O_3/Al_2O_3(T)$ .

dominant species over the surface of the catalyst with the higher calcination temperature, as were shown in Table 2. By comparison, the catalyst  $1.5K_2O-10Cr_2O_3/Al_2O_3(800)$  and the reference catalyst  $1.5K_2O-10Cr_2O_3/Al_2O_3(800)-R$  presented a similar  $Cr^{3+}/Cr^{6+}$  value (1.91 and 1.96, respectively). The surface  $Cr^{3+}$  amount over the catalyst  $1.5K_2O-10Cr_2O_3/Al_2O_3(800)-R$  was 1.56%, which was more than that (1.29%) of the catalyst  $1.5K_2O-10Cr_2O_3/Al_2O_3(800)$ . This meant that the catalyst  $1.5K_2O-10Cr_2O_3/Al_2O_3(800)$  had more inner type of  $Cr^{3+}$  species than the reference catalyst, indicating that the catalyst possessed a more stable support structure [11,41]. In a word, both  $Cr^{3+}$  and  $Cr^{6+}$  species were observed on the surface of the fresh catalysts, their different concentrations were mainly depending on the overall chromia loadings, the promoter  $K_2O$  addition and calcination temperature in this experiment.

### 3.2.5. Diffuse reflectance UV-vis spectra

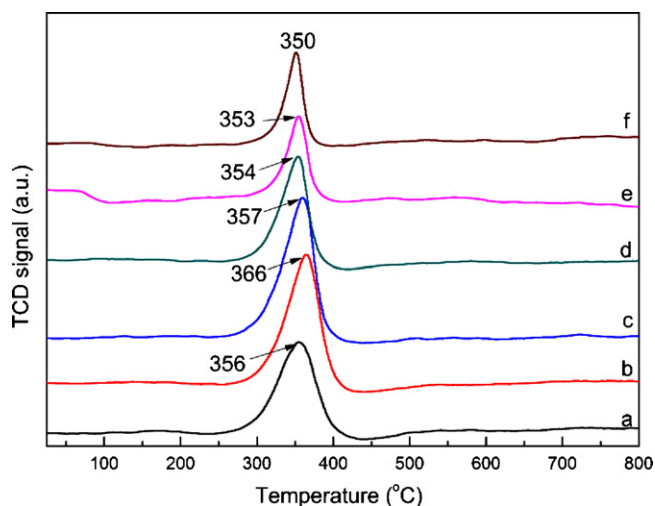
The diffuse reflectance UV-vis spectra of the fresh catalysts  $1.5K_2O-10Cr_2O_3/Al_2O_3(T)$  calcined at different temperatures are plotted in Fig. 3. All spectra exhibited two intense absorption bands at about 271 nm and 366 nm, contributable to  $O^{2-} \rightarrow Cr^{6+}$  charge transfer of chromate species, demonstrating the presence of  $Cr^{6+}$  species on the surface of the catalysts [2,13,39,42,43]. A shoulder peak at 434 nm was assigned to the d-d transition ( $A_{2g} \rightarrow T_{1g}$ ) of  $Cr^{3+}$  species in octahedral symmetry, which band may also derive from

Table 2

The XPS data and the results of isobutane dehydrogenation over the catalysts.

Catalysts	Surface concn. (mol%)		$Cr^{3+}/Cr^{6+}$ (mole ratio)	Activity <sup>a</sup> (mmol g <sup>-1</sup> h <sup>-1</sup> )	TOF <sup>b</sup> (h <sup>-1</sup> )
	Cr	$Cr^{3+}$			
$5Cr_2O_3/Al_2O_3(600)$	1.46	0.83	1.30	12.8	1.54
$10Cr_2O_3/Al_2O_3(600)$	1.78	1.11	1.68	18.3	1.65
$15Cr_2O_3/Al_2O_3(600)$	2.86	1.87	1.90	17.2	0.92
$20Cr_2O_3/Al_2O_3(600)$	3.54	2.38	2.05	17.6	0.74
$25Cr_2O_3/Al_2O_3(600)$	4.81	2.94	1.57	17.3	0.59
$1.5K_2O-10Cr_2O_3/Al_2O_3(500)$	1.95	0.91	0.87	12.9	1.42
$1.5K_2O-10Cr_2O_3/Al_2O_3(600)$	2.01	1.08	1.16	17.5	1.62
$1.5K_2O-10Cr_2O_3/Al_2O_3(700)$	2.04	1.22	1.48	21.5	1.76
$1.5K_2O-10Cr_2O_3/Al_2O_3(800)$	1.96	1.29	1.91	22.4	1.73
$1.5K_2O-10Cr_2O_3/Al_2O_3(900)$	1.96	1.41	2.57	21.4	1.52
$1.5K_2O-10Cr_2O_3/Al_2O_3(800)^c$	1.96	1.29	1.91	29.6	2.30
$1.5K_2O-10Cr_2O_3/Al_2O_3(800)^d$	3.70	3.70	–	–	–
$1.5K_2O-10Cr_2O_3/Al_2O_3(800)^e$	2.04	1.41	2.22	28.3	2.00
$1.5K_2O-10Cr_2O_3/Al_2O_3(800)^f$	2.03	1.40	2.22	29.0	2.07
$1.5K_2O-10Cr_2O_3/Al_2O_3(800)-R^g$	2.36	1.56	1.96	32.2	2.06

<sup>a</sup> Activity was defined as mmol of isobutane converted per gram of catalyst per hour. <sup>b</sup> TOF was defined as number of isobutane converted per  $Cr^{3+}$  site per hour. <sup>c</sup> <sup>d</sup> <sup>e</sup> <sup>f</sup> <sup>g</sup> The activity and TOF stand for the fresh, spent, the first and tenth regenerated catalyst  $1.5K_2O-10Cr_2O_3/Al_2O_3(800)$  and the reference catalyst  $1.5K_2O-10Cr_2O_3/Al_2O_3(800)-R$  over the isobutane dehydrogenation at the GHSV = 1200 h<sup>-1</sup>, respectively.



**Fig. 4.** The  $H_2$ -TPR profiles of (a)  $10Cr_2O_3/Al_2O_3(600)$  and the series catalysts  $1.5K_2O-10Cr_2O_3/Al_2O_3(T)$  calcined at (b)  $500^\circ C$  (c)  $600^\circ C$  (d)  $700^\circ C$  (e)  $800^\circ C$  (f)  $900^\circ C$ .

dichromate/polychromate [24]. An additional weak band at  $581\text{ nm}$  observed for the series catalysts was probably due to another d-d transition ( $A_{2g} \rightarrow T_{2g}$ ) of  $Cr^{3+}$  in octahedral symmetry. The intensity of the latter band in the spectra increased with the increasing calcination temperature. Consequently, the amount of surface  $Cr^{3+}$  species steadily increased with the higher calcination temperature, which was well consistent with XPS results above.

### 3.2.6. $H_2$ -TPR profiles

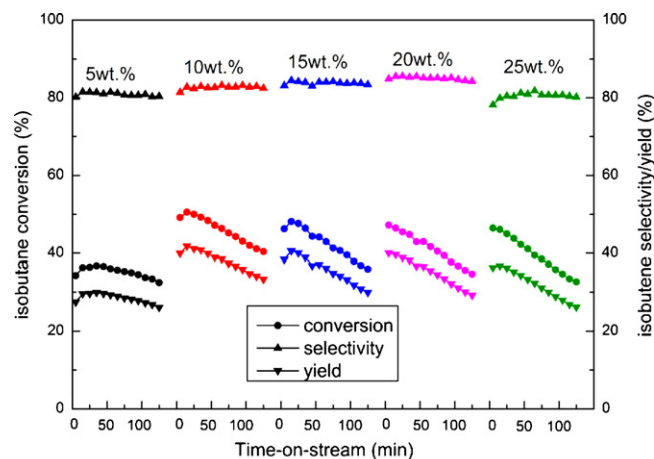
The  $H_2$ -TPR profiles of the studied catalysts are described in Fig. 4. All the samples showed a single  $H_2$  consumption peak ( $T_{max}$ ) at  $350\text{--}366^\circ C$ , corresponding to the reduction of the dispersed  $Cr^{6+}$  to  $Cr^{3+}$  species [20,24,38,44]. The  $T_{max}$  of the catalyst  $10Cr_2O_3/Al_2O_3(600)$  was located at  $356^\circ C$ . By comparison, the similar  $T_{max}$   $357^\circ C$  was observed over the catalyst  $1.5K_2O-10Cr_2O_3/Al_2O_3(600)$ , indicating that the reducibility of the catalyst was independent of the  $K_2O$  addition. It was noteworthy that, moreover, the  $T_{max}$  of the series catalyst  $1.5K_2O-10Cr_2O_3/Al_2O_3(T)$  was a slightly downward shift with the increasing calcination temperature, suggesting that the interaction between  $Cr^{6+}$  and aluminium or oxygen species became weaker at the higher calcination temperature.

### 3.3. Isobutane dehydrogenation

The products observed for isobutane dehydrogenation were mainly isobutene and trace amounts of carbon monoxide, methane, ethane, ethylene, propane, propylene and n-butene besides the unreacted isobutane.

#### 3.3.1. The dehydrogenation reactivity over the catalysts

The reactivity over the series catalysts  $xCr_2O_3/Al_2O_3(600)$  with the increasing TOS for the isobutane dehydrogenation is plotted in Fig. 5. As the  $Cr_2O_3$  loading increased, the initial isobutane conversion and initial isobutene yield increased to the maximum  $49.1\%$  and  $40.0\%$  over the catalyst  $10Cr_2O_3/Al_2O_3(600)$ , then slightly decreased thereafter. Meantime, the initial catalytic activity achieved at its maximum  $18.3\text{ mmol g}^{-1}\text{ h}^{-1}$  (Table 2), demonstrating that the catalyst  $10Cr_2O_3/Al_2O_3(600)$  possessed the highest activity among the series catalysts [45]. It was observed that the highest initial isobutene selectivity  $84.9\%$  was obtained over the catalyst  $20Cr_2O_3/Al_2O_3(600)$ . For each catalyst, moreover, the isobutane conversion and isobutene yield gradually reduced with



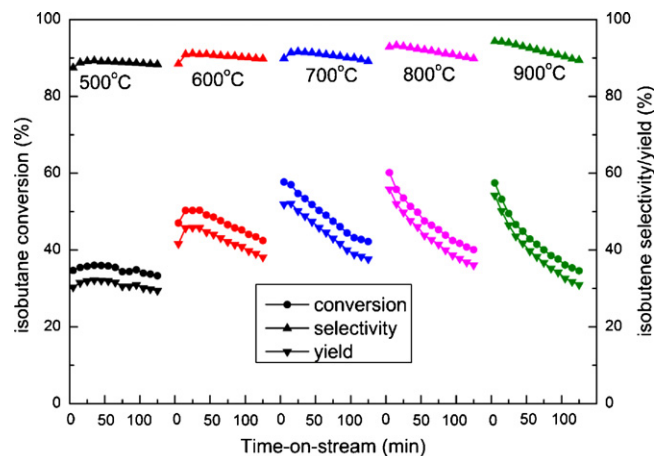
reaction conditions:  $T = 600^\circ C$ , catalyst:  $0.60\text{ g}$ , GHSV =  $833\text{ h}^{-1}$ ,  $t = 2\text{ h}$ .

**Fig. 5.** The reactivity of the isobutane dehydrogenation over the series catalysts  $xCr_2O_3/Al_2O_3$ .

the increasing reaction time, which was due to the coke formation over the catalyst [3,9,14,46]. It was not difficult to notice that the isobutane conversion and isobutene yield of the catalyst with lower  $Cr_2O_3$  loading decreased more slightly than that of the catalyst with higher  $Cr_2O_3$  loading during the dehydrogenation reaction, demonstrating that the catalyst  $5Cr_2O_3/Al_2O_3(600)$  exhibited much higher stability among the series catalysts over the dehydrogenation.

The catalytic reactivity over the series catalysts  $1.5K_2O-10Cr_2O_3/Al_2O_3(T)$  for the isobutane dehydrogenation are shown in Fig. 6. By comparison with the catalyst  $10Cr_2O_3/Al_2O_3(600)$ , the isobutane conversion had no significant increase over the K-doped catalyst  $1.5K_2O-10Cr_2O_3/Al_2O_3(600)$ . Nevertheless, the isobutene selectivity greatly increased by  $7.1\text{--}8.1\%$ , indicating that potassium was an effective promoter to the catalytic selectivity. Moreover, it was observed that the isobutane conversion and isobutene selectivity of the K-doped catalyst decreased more slightly than that of the catalyst  $10Cr_2O_3/Al_2O_3(600)$ , indicating that the deactivation rate of the catalyst was greatly suppressed by  $K_2O$  addition. The similar effect of  $K_2O$  over the dehydrogenation was reported by the previous literatures [6,14,16,20,21].

As for the influence of calcination temperature over the dehydrogenation reactivity (Fig. 6), the initial isobutane conversion and initial isobutene yield increased to the maximum  $60.1\%$



reaction conditions:  $T = 600^\circ C$ , catalyst:  $0.60\text{ g}$ , GHSV =  $833\text{ h}^{-1}$ ,  $t = 2\text{ h}$ .

**Fig. 6.** The reactivity of the isobutane dehydrogenation over the series catalysts  $1.5K_2O-10Cr_2O_3/Al_2O_3(T)$ .

and 56.1% over the catalyst  $1.5 \text{ K}_2\text{O}-10\text{Cr}_2\text{O}_3/\text{Al}_2\text{O}_3(800)$ . Simultaneously, the catalyst exhibited the optimum initial catalytic activity  $22.4 \text{ mmol g}^{-1} \text{ h}^{-1}$  among the series catalysts. It was observed that the initial isobutene selectivity was up to 93.2% over the catalyst calcined at  $800^\circ\text{C}$ . With the increasing calcination temperature, the initial isobutene selectivity increased and achieved at the maximum 94.3% over the catalyst  $1.5 \text{ K}_2\text{O}-10\text{Cr}_2\text{O}_3/\text{Al}_2\text{O}_3(900)$ . Moreover, it was obviously noticed that the isobutane conversion and isobutene yield over the catalyst calcined at higher temperature decreased more quickly during the reaction, indicating that the catalyst calcined at lower temperature was more stable over the dehydrogenation. Also, the decreased isobutane conversion and isobutene yield of each catalyst with the increase of the TOS over the dehydrogenation was assigned to the coke deposition over the catalyst [3,9,14,46].

### 3.3.2. The active chromium species

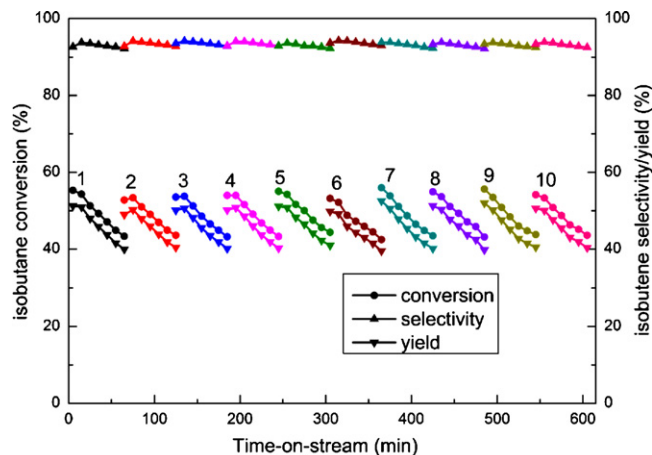
In case of the valence of the active chromium species, the active species in dehydrogenation is  $\text{Cr}^{3+}$ , or both  $\text{Cr}^{3+}$  and  $\text{Cr}^{2+}$ , or coordinative unsaturated  $\text{Cr}^{3+}$  according to the previous literatures [1,4,5,7,14,47–49]. Therefore, it is still an open question in the literatures. In our experiment, it was suggested that  $\text{Cr}^{3+}$  was mainly the active site for isobutane dehydrogenation and the isobutene selectivity was depended on the surface  $\text{Cr}^{3+}/\text{Cr}^{6+}$  value over the catalyst.

Table 2 clearly shows the catalytic activity of isobutane dehydrogenation over the catalysts. With regard to the series catalysts  $x\text{Cr}_2\text{O}_3/\text{Al}_2\text{O}_3(600)$ , it was observed that the catalytic activity increased with the increasing surface  $\text{Cr}^{3+}$  amount over the catalyst with chromia loading up to 10 wt.%. The catalyst  $x\text{Cr}_2\text{O}_3/\text{Al}_2\text{O}_3(600)$  with chromia loading more than 15 wt.% exhibited the lower catalytic activity than the catalyst  $10\text{Cr}_2\text{O}_3/\text{Al}_2\text{O}_3(600)$ , which was ascribed to the larger and lower dispersed chromia particles over the these catalysts, consistent with the PXRD results. It was observed that the isobutene selectivity increased with the increasing  $\text{Cr}^{3+}/\text{Cr}^{6+}$  value over the series catalysts  $x\text{Cr}_2\text{O}_3/\text{Al}_2\text{O}_3(600)$ , agreement with the XPS results. For the series K-doped catalysts calcined at different temperatures, the catalytic activity increased with the increasing surface  $\text{Cr}^{3+}$  amount over the catalysts. The slightly decreased activity over the K-doped catalyst calcined at  $900^\circ\text{C}$  was probably assigned to the appearance of  $\alpha\text{-Al}_2\text{O}_3$  in the support and low specific surface area of the catalyst. Moreover, the isobutene selectivity increased with increasing  $\text{Cr}^{3+}/\text{Cr}^{6+}$  value over the series catalysts.

Based on these results and the data in Table 2, we concluded that the catalytic activity was improved with the increase of surface  $\text{Cr}^{3+}$  amount over the catalyst with highly dispersed chromium species and the isobutene selectivity was enhanced with the increasing surface  $\text{Cr}^{3+}/\text{Cr}^{6+}$  value. In addition, the TOF (turnover frequency) over the catalysts with highly dispersed chromium species were  $1.6 \pm 0.2 \text{ h}^{-1}$ . This meant that the activity per  $\text{Cr}^{3+}$  site over the catalysts was almost the same. Analogously, De Rossi et al. found that the activity per atom of chromium was the same over the Cr-based catalysts with different chromia loadings [47]. Lugo and Lunsford also observed the same turnover frequency over the unsupported and supported chromium oxide catalysts [50].

### 3.3.3. The dehydrogenation-regeneration cycles of the catalyst

In order to examine the regenerative ability and stability of the catalyst during the isobutane dehydrogenation, the ten dehydrogenation-regeneration cycles over the catalyst  $1.5 \text{ K}_2\text{O}-10\text{Cr}_2\text{O}_3/\text{Al}_2\text{O}_3(800)$  were investigated (Fig. 7). It was calculated that the initial isobutane conversion, isobutene selectivity and yield were 55.3%, 92.7% and 51.3% in the first cycle, respectively. In the tenth cycle, by comparison, the initial isobutane conversion, isobutene selectivity and yield were 54.2%, 93.4% and 50.6%,



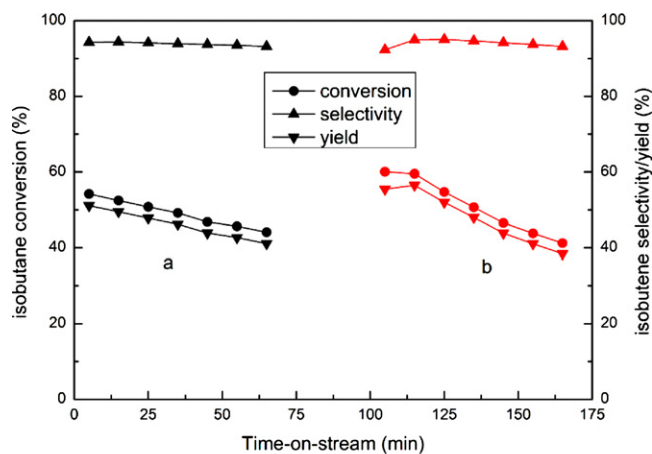
Reaction conditions:  $T = 600^\circ\text{C}$ , catalyst: 0.60 g, GHSV =  $1200 \text{ h}^{-1}$ ,  $t = 1 \text{ h}$ .

Fig. 7. The ten dehydrogenation-regeneration cycles of the isobutane dehydrogenation over the catalyst  $1.5 \text{ K}_2\text{O}-10\text{Cr}_2\text{O}_3/\text{Al}_2\text{O}_3(800)$ .

respectively. Moreover, it was calculated that the catalytic activity was  $29.6 \text{ mmol g}^{-1} \text{ h}^{-1}$  in the first cycle and  $29.0 \text{ mmol g}^{-1} \text{ h}^{-1}$  in the tenth cycle, which was maintainable during the ten cycles (Table 2). The basically unchanged activity and selectivity during the ten dehydrogenation-regeneration cycles indicated the high regenerative ability and high stability of the catalyst.

### 3.3.4. The comparison of the activity with the reference catalyst

The catalyst  $1.5 \text{ K}_2\text{O}-10\text{Cr}_2\text{O}_3/\text{Al}_2\text{O}_3(800)$  was compared with the catalyst  $1.5 \text{ K}_2\text{O}-10\text{Cr}_2\text{O}_3/\text{Al}_2\text{O}_3(800)\text{-R}$  prepared by impregnation method over the isobutane dehydrogenation (Fig. 8). It was observed that the reference catalyst exhibited a slightly higher initial isobutane conversion and comparable isobutene selectivity (about 94.0%) by contrast with the catalyst  $1.5 \text{ K}_2\text{O}-10\text{Cr}_2\text{O}_3/\text{Al}_2\text{O}_3(800)$ . This was probably assigned to that the reference catalyst presented more surface  $\text{Cr}^{3+}$  species and comparable  $\text{Cr}^{3+}/\text{Cr}^{6+}$  value with the catalyst  $1.5 \text{ K}_2\text{O}-10\text{Cr}_2\text{O}_3/\text{Al}_2\text{O}_3(800)$ , in accordance with the XPS characterization. However, the isobutane conversion and isobutene yield of the reference catalyst decreased more rapidly compared with the catalyst  $1.5 \text{ K}_2\text{O}-10\text{Cr}_2\text{O}_3/\text{Al}_2\text{O}_3(800)$ , indicating that the catalyst  $1.5 \text{ K}_2\text{O}-10\text{Cr}_2\text{O}_3/\text{Al}_2\text{O}_3(800)$  possessed a more stable activity during the dehydrogenation. It may be due to the stabilization of the



Reaction conditions:  $T = 600^\circ\text{C}$ , catalyst: 0.60 g, GHSV =  $1200 \text{ h}^{-1}$ ,  $t = 1 \text{ h}$ .

Fig. 8. The reactivity of isobutane dehydrogenation over the catalyst (a)  $1.5 \text{ K}_2\text{O}-10\text{Cr}_2\text{O}_3/\text{Al}_2\text{O}_3(800)$  and (b)  $1.5 \text{ K}_2\text{O}-10\text{Cr}_2\text{O}_3/\text{Al}_2\text{O}_3(800)\text{-R}$ .

support structure of the inner Cr<sup>3+</sup> species in the catalyst 1.5 K<sub>2</sub>O-10Cr<sub>2</sub>O<sub>3</sub>/Al<sub>2</sub>O<sub>3</sub>(800) at calcination [11,41].

### 3.4. The characterizations of spent and regenerated catalysts

#### 3.4.1. N<sub>2</sub> adsorption-desorption measurements

The BET specific surface areas and pore properties of the spent and regenerated catalysts are presented in Table 1. Compared with the fresh catalyst, the spent one had a slightly smaller specific surface area 190.9 m<sup>2</sup> g<sup>-1</sup>, lower pore volume 0.65 cm<sup>3</sup> g<sup>-1</sup> and smaller pore size 12.28 nm. The reason for this was probably due to that coke deposition on the spent catalyst inhibited a portion of the pore, thus leading to the slight decrease in the textural performance of the catalyst. During the ten dehydrogenation-regeneration cycles, the basically invariant specific surface area (177.9 → 172.1 m<sup>2</sup> g<sup>-1</sup>) and pore volume (0.55 → 0.53 cm<sup>3</sup> g<sup>-1</sup>) of the regenerated catalyst from the first to tenth cycle demonstrated its high stability of the catalyst.

#### 3.4.2. PXRD patterns

Fig. 2B displays the PXRD patterns of the spent and the tenth regenerated catalyst 1.5 K<sub>2</sub>O-10Cr<sub>2</sub>O<sub>3</sub>/Al<sub>2</sub>O<sub>3</sub>(800). It was observed that no potassium and chromia phases appeared in the PXRD pattern of the corresponding spent catalyst, implying that the reaction conditions had no significant influence over the dispersion of these species. The potassium and chromia phases were not visible over the tenth regenerated catalyst, demonstrating the high phase stability of the catalysts during the ten cycles over the isobutane dehydrogenation.

#### 3.4.3. TEM images

The TEM images of the spent catalysts are presented in Fig. 3g–i. The worm-like mesopores of the spent catalysts suggested that the pores were non-ordered, which were very similar to that of the corresponding fresh catalysts. It was clearly seen that no chromia particles were on the surface of the alumina support, indicating its high dispersion over the spent catalysts. These results implied again the high stability of the catalyst, which was in good agreement with the N<sub>2</sub> adsorption-desorption and PXRD characterizations. Moreover, the morphology of the carbon residues was not clearly observed on the spent catalysts, indicating the carbon residues were amorphous.

#### 3.4.4. XPS spectra

The XPS data of the spent and regenerated catalyst 1.5 K<sub>2</sub>O-10Cr<sub>2</sub>O<sub>3</sub>/Al<sub>2</sub>O<sub>3</sub>(800) are presented in Table 2. Compared with the fresh catalyst, it was observed that only Cr<sup>3+</sup> species were over the spent catalyst, indicating that Cr<sup>6+</sup> species was reduced by the reaction molecules. Moreover, the amounts of surface potassium and chromium species both increased largely over the spent catalyst, which was probably due to the decrease of the specific surface area led to the low dispersion of the two species over the surface of the catalyst. After re-calcination in air, the Cr<sup>6+</sup> species were observed over the regenerated catalyst, suggesting that a portion of Cr<sup>3+</sup> species were oxidized to Cr<sup>6+</sup> in the re-calcination process. The invariantly unchanged amount of Cr<sup>3+</sup> species (1.41% → 1.40%) and Cr<sup>3+</sup>/Cr<sup>6+</sup> value (2.22 → 2.22) were responsible for the maintainable activity and selectivity during the ten dehydrogenation-regeneration cycles.

## 4. Conclusions

In summary, the no-ordered mesoporous Cr<sub>2</sub>O<sub>3</sub>/Al<sub>2</sub>O<sub>3</sub> catalysts with large specific surface areas (149.4–381.6 m<sup>2</sup> g<sup>-1</sup>) and high pore volume (0.77–1.24 cm<sup>3</sup> g<sup>-1</sup>) were successfully synthesized from a Cr-based MOF material MIL-101 as the molecular

host and chromium precursor. The reactivity of isobutane dehydrogenation was investigated over the catalysts. The pore texture, structural phase, the reducibility and the surface concentrations of Cr<sup>3+</sup> and Cr<sup>6+</sup> species over the catalysts were depending on the chromia loadings and calcination temperature. The K<sub>2</sub>O addition to the catalyst slightly decreased the specific surface area and the surface Cr<sup>3+</sup>/Cr<sup>6+</sup> value. However, it greatly improved the isobutene selectivity and reduced the deactivation rate. The catalyst 1.5 K<sub>2</sub>O-10Cr<sub>2</sub>O<sub>3</sub>/Al<sub>2</sub>O<sub>3</sub>(800) calcined at 800 °C exhibited high isobutene selectivity up to 93.2% at the highest isobutane conversion of 60.1%. The catalytic activity increased with the increasing amount of Cr<sup>3+</sup> species over the catalysts with highly dispersed chromium species and the catalytic selectivity was enhanced with the increasing surface Cr<sup>3+</sup>/Cr<sup>6+</sup> value of the catalyst. The maintainable activity and selectivity over isobutane dehydrogenation in the ten dehydrogenation-regeneration cycle demonstrated the very high stability and regenerative ability of the catalyst. Compare with the catalyst prepared by impregnation method, the catalyst in this work presented more stable activity in the dehydrogenation. This study presents a feasible way to facile synthesis of the Cr<sub>2</sub>O<sub>3</sub>/Al<sub>2</sub>O<sub>3</sub> catalysts with good catalytic performance and high stability from a MOF material.

## Acknowledgement

We gratefully acknowledge the financial support of the State Key Laboratory for Oxo Synthesis and Selective Oxidation of China and Suzhou Science and Technology Bureau of Applied Foundation Research Project (SYG201219).

## References

- [1] S. De Rossi, G. Ferraris, S. Fremiotti, V. Indovina, A. Cimino, Appl. Catal. A: Gen. 106 (1993) 125–141.
- [2] F. Cavani, M. Koutyrev, F. Trifirò, A. Bartolini, D. Ghisletti, R. Iezzi, A. Santucci, G.D. Piero, J. Catal. 158 (1996) 236–250.
- [3] S.M. Stagg, C.A. Querini, W.E. Alvarez, D.E. Resasco, J. Catal. 168 (1997) 75–94.
- [4] B.M. Weckhuysen, A.A. Verberckmoes, J. Debaere, K. Ooms, I. Langhans, R.A. Schoonheydt, J. Mol. Catal. A: Chem. 151 (2000) 115–131.
- [5] A.B. Gaspar, L.C. Dieguez, J. Catal. 220 (2003) 309–316.
- [6] M. Tasbihi, F. Feyzi, M.A. Amlashi, A.Z. Abdullah, A.R. Mohamed, Fuel Process. Technol. 88 (2007) 883–889.
- [7] A. Hakuli, A. Kytökiivi, A.O.I. Krause, Appl. Catal. A: Gen. 190 (2000) 219–232.
- [8] S. Wang, K. Murata, T. Hayakawa, S. Hamakawa, K. Suzuki, Appl. Catal. A: Gen. 196 (2000) 1–8.
- [9] J. Gascón, C. Téllez, J. Herguido, M. Menéndez, Appl. Catal. A: Gen. 248 (2003) 105–116.
- [10] R.G. Craig, J.M. Dufallo, Chem. Eng. Prog. 75 (1979) 62–65.
- [11] E.I. Nemykina, N.A. Pakhomov, V.V. Danilevich, V.A. Rogov, V.I. Zaikovskii, T.V. Larina, V.V. Molchanov, Kinet. Catal. 51 (2010) 898–906.
- [12] S. Udonsak, R.G. Anthony, Ind. Eng. Chem. Res. 35 (1996) 47–53.
- [13] S. De Rossi, M.P. Casaleto, G. Ferraris, A. Cimino, G. Minelli, Appl. Catal. A: Gen. 167 (1998) 257–270.
- [14] B.M. Weckhuysen, R.A. Schoonheydt, Catal. Today 51 (1999) 223–232.
- [15] S.T. Korhonen, S.M.K. Airaksinen, M.A. Bañares, A.O.I. Krause, Appl. Catal. A: Gen. 333 (2007) 30–41.
- [16] R.D. Cortright, J.A. Dumesic, J. Catal. 157 (1995) 576–583.
- [17] J.M. Hill, R.D. Cortright, J.A. Dumesic, Appl. Catal. A: Gen. 168 (1998) 9–21.
- [18] Y.K. Park, F.H. Ribeiro, G.A. Somorjai, J. Catal. 178 (1998) 66–75.
- [19] B. Grzybowska-Świerkosz, Top. Catal. 21 (2002) 35–46.
- [20] E. Rombi, M.G. Cutrufello, V. Solinas, S. De Rossi, G. Ferraris, A. Pistone, Appl. Catal. A: Gen. 251 (2003) 255–266.
- [21] G.J. Siri, G.R. Bertolini, M.L. Casella, O.A. Ferretti, Mater. Lett. 59 (2005) 2319–2324.
- [22] J. Słoczyński, B. Grzybowska, A. Kozłowska, K. Samson, R. Grabowski, A. Kotarba, M. Hermanowska, Catal. Today 169 (2011) 29–35.
- [23] S.M.K. Airaksinen, A.O.I. Krause, Ind. Eng. Chem. Res. 44 (2005) 3862–3868.
- [24] D. Shee, A. Sayari, Appl. Catal. A: Gen. 389 (2010) 155–164.
- [25] Y. Echegoyen, I. Suelves, M.J. Lázaro, M.L. Sanjuán, R. Moliner, Appl. Catal. A: Gen. 333 (2007) 229–237.
- [26] M.J. Lázaro, Y. Echegoyen, C. Alegre, I. Suelves, R. Moliner, J.M. Palacios, Int. J. Hydrogen Energy 33 (2008) 3320–3329.
- [27] M.A. Ermakova, D.Y. Ermakov, G.G. Kuvshinov, L.M. Plyasova, J. Catal. 187 (1999) 77–84.
- [28] G. Férey, C. Mellot-Draznieks, C. Serre, F. Millange, J. Dutour, S. Surblé, I. Margiolaki, Science 309 (2005) 2040–2042.

- [29] O.I. Lebedev, F. Millange, C. Serre, G.V. Tendeloo, G. Férey, *Chem. Mater.* 17 (2005) 6525–6527.
- [30] M. Latroche, S. Surblé, C. Serre, C. Mellot-Draznieks, P.L. Llewellyn, J.H. Lee, J.S. Chang, S.H. Jhung, G. Férey, *Angew. Chem. Int. Ed.* 45 (2006) 8227–8231.
- [31] P.L. Llewellyn, S. Bourrelly, C. Serre, A. Vimont, M. Daturi, L. Hamon, G.D. Weireld, J.-S. Chang, D.-Y. Hong, Y.K. Hwang, S.H. Jhung, G. Férey, *Langmuir* 24 (2008) 7245–7250.
- [32] B. Liu, H. Shioyama, T. Akita, Q. Xu, *J. Am. Chem. Soc.* 130 (2008) 5390–5391.
- [33] R.K. Bhakta, J.L. Herberg, B. Jacobs, A. Highley, J.R. Behrens, N.W. Ockwig, J.A. Greathouse, M.D. Allendorf, *J. Am. Chem. Soc.* 131 (2009) 13198–13199.
- [34] W.X. Wang, Y.W. Li, R.J. Zhang, D.H. He, H.L. Liu, S.J. Liao, *Catal. Commun.* 12 (2011) 875–879.
- [35] R. Das, P. Pachfule, R. Banerjee, P. Poddar, *Nanoscale* 4 (2012) 591–599.
- [36] A. Henschel, K. Gedrich, R. Kraehnert, S. Kaskel, *Chem. Commun.* (2008) 4192–4194.
- [37] H. Lu, D.H. Shen, C.L. Bao, Y.X. Wang, *Phys. Status Solidi A* 159 (1997) 425–437.
- [38] B. Grzybowska, J. Słoczyński, R. Grabowski, K. Wcisło, A. Kozłowska, J. Stoch, J. Zieliński, *J. Catal.* 178 (1998) 687–700.
- [39] T.V.M. Rao, E.M. Zahidi, A. Sayari, *J. Mol. Catal. A: Chem.* 301 (2009) 159–165.
- [40] G. Wang, L. Zhang, J. Deng, H. Dai, H. He, C.T. Au, *Appl. Catal. A: Gen.* 355 (2009) 192–201.
- [41] N.V. Vernikovskaya, I.G. Savin, V.N. Kashkin, N.A. Pakhomov, A. Ermakova, V.V. Molchanov, E.I. Nemykina, O.A. Parahin, *Chem. Eng. J.* 176–177 (2011) 158–164.
- [42] S. Khaddar-Zine, A. Ghorbel, C. Naccache, *J. Mol. Catal. A: Chem.* 150 (1999) 223–231.
- [43] M. Cherian, M.S. Rao, A.M. Hirt, I.E. Wachs, G. Deo, *J. Catal.* 211 (2002) 482–495.
- [44] J.M. Kanervo, A.O.I. Krause, *J. Catal.* 207 (2002) 57–65.
- [45] M. Boudart, *Chem. Rev.* 95 (1995) 661–666.
- [46] T. Matsuda, I. Koike, N. Kubo, E. Kikuchi, *Appl. Catal. A: Gen.* 96 (1993) 3–13.
- [47] S. De Rossi, G. Ferraris, S. Fremiotti, A. Cimino, V. Indovina, *Appl. Catal. A: Gen.* 81 (1992) 113–132.
- [48] A. Hakuli, M.E. Harlin, L.B. Backman, A.O.I. Krause, *J. Catal.* 184 (1999) 349–356.
- [49] R. Puurunen, B.E. Weckhuysen, *J. Catal.* 210 (2002) 418–430.
- [50] H.J. Lugo, J.H. Lunsford, *J. Catal.* 91 (1985) 155–166.